ISBN: 978-3-95450-214-1 ISSN: 2673-5490 doi:10.18429/JACoW-IPAC2021-THPAB083

MEASUREMENT OF THE LONGITUDINAL PHASE-SPACE OF THE APS PHOTO-INJECTOR BEAM*

Yine Sun†, Argonne National Lab., Lemont, Illinois, USA

Abstract

While the primary beam of the Argonne Advanced Photon Source (APS) linac is generated by a thermionic rf gun to support the APS storage ring user operation, an S-band photo-cathode RF gun (PCG) exists at the front of the linac. The high-brightness photoinjector beam is accelerated by the linac and and can be used for accelerator technology and beam physics R&D experiments in the Linac Extension Area (LEA). For some applications, the beam needs to be compressed by a magnetic bunch compressor in the middle of the linac. An S-band transverse-mode cavity (Tcav) is available at the end of the linac for beam longitudinal phase-space diagnostics. Beam commissioning experience of the Tcav is reported in this paper. The cavity rf conditioning and calibration was performed. There is a horizontally bending dipole magnet downstream of the Tcav, which kicks beam in the vertical plane. Beam image on a YAG screen downstream of the Tcav and dipole magnet contains the single-shot information of the longitudinal phase-space of the photo-injector beam. The first measurements of the longitudinal phase-space of the compressed and non-compressed photoinjector beam are discussed. Improvements of the measurement resolution are planned, as the existing beam imaging system were not designed for longitudinal phase-space measurements.

INTRODUCTION

An S-band PCG was commissioned at the Injector Test Stand at APS [1]. The gun was later installed at the frontend of the APS linac as shown in Fig. 1. Beam generated by the PCG is accelerated through the linac, in which thirteen 3-meter long S-band accelerating structures boost beam energy to 425 MeV. The first sector, L1, has only one accelerating strucgure, while each of the other three sectors (L2, L4, and L5) has four structures. Sector L3 is composed of four dipole magnets which form a chicane for bunch compression [2]. A sketch of the linac is shown in Fig. 2. After the linac, the PCG beam can be either injected into the Particle Accumulator Ring (PAR), or it can remain on a straight path directed to LEA.

A 13-cell LOLA-type traveling wave deflecting cavity was installed at the end of the linac, see Fig. 3. The cavity streaks beam in the vertical direction. A maximum input rf power of 19 MW was reached at the end of the rf conditioning, which corresponds to a deflecting voltage of 3.8 MV according to Eq. (1) [3].

* Work supported by the U.S. Department of Energy, Office of Science, Office of Basic Energy Sciences, under Contract No. DE-AC02-06CH11357.
† yinesun@anl.gov

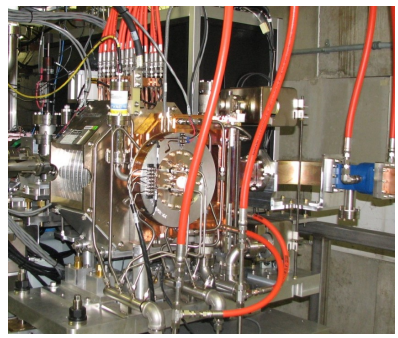

Figure 1: The PCG, its bucking solenoid and main solenoid, are installed in the frontend of the linac.

$$V[\mathrm{MV}] = k_D L[\mathrm{m}]\sqrt{P[\mathrm{MW}]}, \quad (1)$$

where V is the deflecting voltage in MV, the deflecting stregth k_D equals to 1.63 MV/m/$\sqrt{\mathrm{MW}}$, the deflecting cavity length L[m] is 0.53 m, and P is the input power in MW.

SETUP LINAC FOR PC GUN BEAM

Normally the APS linac is occupied by thermionic RF gun beams for injection into the PAR. During machine studies, the linac can be setup for PCG beam. The RF phase of the PCG is set to 40° from zero-crossing of the phase scan. Beam is accelerated to a final energy of 425 MeV through the linac. The RF phase of the linac sectors is initially set for minimum energy spread. It requires 10's of minutes to slowly bring up the RF power to 19 MW in the Tcav whenever the low level RF is turned off for machine protection purposes. To avoid turning on and off the Tcav during the experiment, the LLRF gate start time of the rf source is adjusted so that electron beam either sees or misses the RF field on the Tcav as needed.

MEASUREMENT OF THE PCG BEAM LONGITUDINAL PHASE-SPACE

Two flags downstream of the Tcav are can be used for the measurement of beam longitudinal phase-space properties, one in the straight ahead beam line (FL3), and one in a dipole magnet bend line (FL1), see Fig. 2 for flag locations. Tcav forward power is set at 19 MW. With linac RF phase set at minimum energy spread, beam on FL3 is shown in Fig. 4. Beam vertical rms size is stretched from 2.4 pixels to 12.1 pixels when Tcav power is changed from zero to 19 MW.

Adjusted the linac sector L2 RF phase to introduce a correlated energy spread for bunch compression using the L3 chicane. Meanwhile the gradient of L2 is also increased

ISBN: 978-3-95450-214-1 ISSN: 2673-5490 doi:10.18429/JACoW-IPAC2021-THPAB083

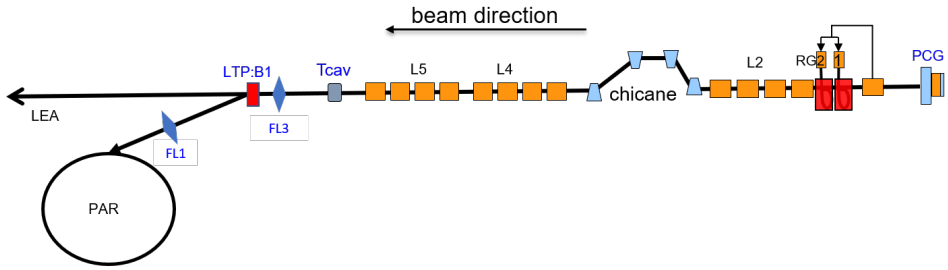

Figure 2: A sketch of the APS linac beamline.

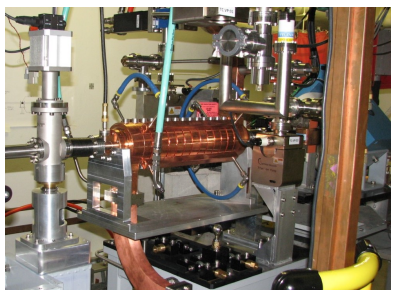

Figure 3: A 13-cell transverse-mode rf cavity was installed at the end of the linac.

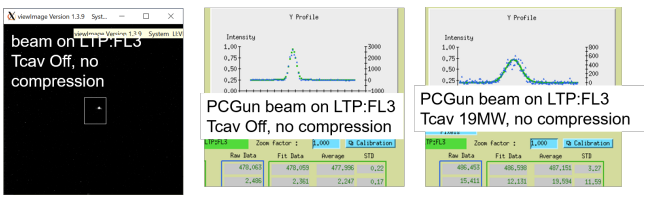

Figure 4: PCG beam on FL3 without bunch compression.

to maintain the same beam energy at the chicane. With Tcav off, rms vertical beam size on FL3 is 1.8 pixels with linac lattice set to achieve a minimal vertical rms beam size; and with Tcav at 19 MW RF power and zero-crossing RF phase, the it is increased to 2.2 pixels, see Fig. 5.

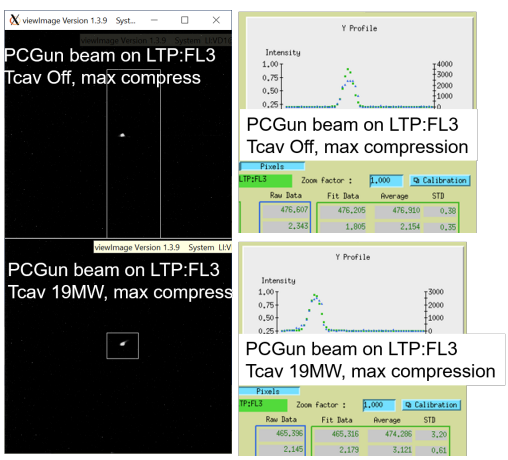

Figure 5: PCG beam on FL3 with bunch compression.

For a complete single-shot longitudinal phase-space measurements, the flag FL1 in the dispersive beamline downstream of the dipole magnet is used. While the vertically deflecting Tcav casts the time-domain information on the vertical direction on the flag, the LTP:B1 horizontally bends the beam thus projecting the energy domain information on the horizontal direction on the flag. The vertical beam size on FL1 with Tcav off is 4.5 pixels and Tcav at 19 MW is 5.9 pixels, see Fig. 6.

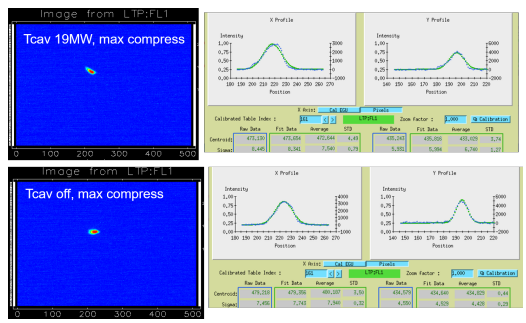

Figure 6: PCG beam on FL1 with bunch compression.

After adjusting the LTP lattice, the difference of the vertical beam size on FL1 with Tcav on and off is increased to a factor of two – 2. 9 pixels with Tcav off, and 6.1 pixels with Tcav on, see Fig. 7.

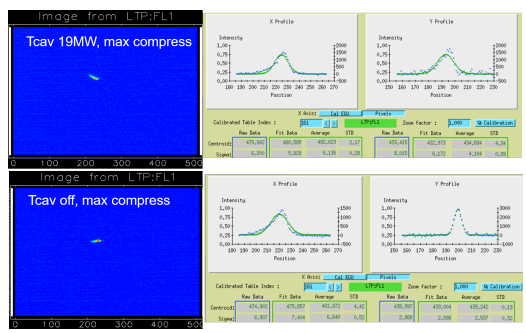

Figure 7: PCG beam on FL1 with bunch compression with adjusted lattice.

Returning L2 sector phase and gradient for minimum energy spread, i.e., no bunch compression, we see that vertical beam rms size on FL1 is increased by a factor of 5, from 6.1 pixels of the compressed beam (Fig. 7) to 30.5 pixels, as shown in Fig. 8. The S-band RF curvature is visible on the screen with Tcav at 19 MW as the linac is phased for minimum energy spread.

ISBN: 978-3-95450-214-1 ISSN: 2673-5490 doi:10.18429/JACoW-IPAC2021-THPAB083

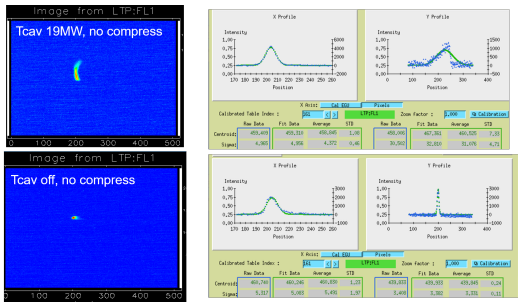

Figure 8: PCG beam on FL1 without bunch compression with adjusted lattice.

SUMMARY

Beam image on FL1 contains the single-shot information of the longitudinal phase-space of the PCG beam, a summary of the beam images taken at different machine conditions are collected in Fig. 9 for comparison purpose.

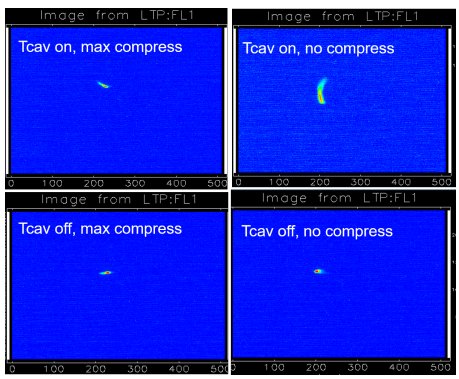

Figure 9: Beam on FL1 with Tcav on/off and with/without compression.

Quadratically subtract the Tcav-off rms beam size from the Tcav-on beam size (see Table 1), we find the beam size induced by the Tcav which is linearly correlated to the rms bunch length. A calibration factor is obtained to convert rms vertical beam size in pixels to rms bunch length in rf degrees, and for S-band 2856 MHz RF, we have 0.97 ps/deg. The calibration is obtained by scanning the Tcav RF phase near the zero-crossing and measure beam centroid motion on FL1, see Fig. 10.

Table 1: Vertical Rms Beam Size with Tcav On/Off and with/without Compression

Compression	Yes	No
Tcav On	6.1	30.5
Tcav Off	2.9	3.4

Using a factor of 0.16 ps/deg for linac setup close to maximum compression, and 0.22 deg/pixel for minimum energy spread case, the bunch lengths are obtained for the PCG beam with and without compression, as listed in Table 2.

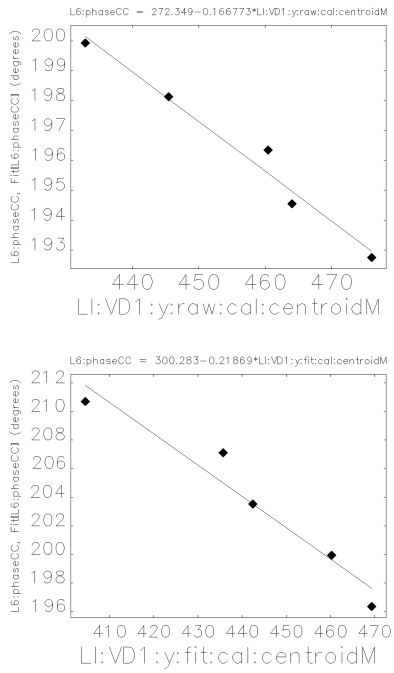

Figure 10: Tcav streaking strength calibration on FL1 with (top) and without compression (bottom).

Table 2: Vertical Rms Bunch Length with/without Compression

Compression	Yes	No
σ_t (ps)	0.86	6.4

For better measurement resolution, we need to improve the imaging system resolution at FL1. As we can see from Fig. 9, beam image only occupies a small portion of the imaging frame – the camera needs to zoom in on the beam. Additionally, diagnostics lattice can be better optimized to improve both time and energy domain measurements, both numerically and experimentally.

REFERENCES

[1] Y.-E. Sun *et al.*, "Commissioning of the Photo-Cathode RF Gun at APS", in *Proc. 36th Int. Free Electron Laser Conf. (FEL'14)*, Basel, Switzerland, Aug. 2014, paper THP039, pp. 803–806.

[2] M. Borland, "Design and performance simulations of the bunch compressor for the Advanced Photon Source Low-Energy Undulator Test Line free-electron laser", *Phys. Rev. ST Accel. Beams*, vol. 4, p. 074201, 2001. doi:10.1103/PhysRevSTAB.4.074201

[3] D. Hui *et al.*, "Numerical study and test of the APS linac transverse deflecting cavity", *Nucl. Instrum. Methods Phys. Res., Sect. A*, vol. 923, pp. 118–126, 2019. doi:10.1016/j.nima.2019.01.043